

**A NARROWBAND PHOTON PAIR SOURCE FOR
QUANTUM COMMUNICATION APPLICATIONS**

PEH YU XIANG

**ENGINEERING SCIENCE PROGRAMME
NATIONAL UNIVERSITY OF SINGAPORE**

2020/2021

**A NARROWBAND PHOTON PAIR SOURCE
FOR QUANTUM COMMUNICATION
APPLICATIONS**

PEH YU XIANG

**A THESIS SUBMITTED FOR THE DEGREE OF
BACHELOR OF ENGINEERING
ENGINEERING SCIENCE PROGRAMME
NATIONAL UNIVERSITY OF SINGAPORE**

Acknowledgements

Firstly, a small shoutout to the #01-05 sofa who has quietly kept me, and the many generations before me, company during many sleepless nights.

Much credit for my technical skill in the lab today is attributed to my project mentor Lijiong who has tirelessly guided me through the many setbacks along the way, and without whom the project would have never seen (1310 nm) light. A big thank you!

I am also grateful to Prof. Christian Kurtsiefer for the opportunity to work on the project, and for being a huge source of inspiration when it comes to learning everything under the sun.

To the many others in the Quantum Optics group, especially Adrian, Pengkian, Xijie, Jianwei et al. Thank you for the many banter, technical help and meaningful conversations that kept my soul afloat in the office.

Last but not least, my parents as well as my dearest Jazreel, who probably don't understand a thing I do in the lab, but have been my greatest personal source of strength to carry on anyway.

Table of Contents

1	Introduction	1
1.1	Narrowband photon pair source	1
1.2	SPDC for quantum communication	1
1.3	Outline of thesis	4
2	Preliminaries	5
2.1	Spontaneous parametric down-conversion	5
2.1.1	Heralded photon source	5
2.1.2	Phase matching	6
2.1.3	Quasi-phase matching	8
2.1.4	Non-degenerate photon pairs	9
2.2	Detection of photon pairs	10
2.2.1	Single photon detection	10
2.2.2	Spectral bandwidth measurement	12
3	Experimental results	13
3.1	Type-II SPDC	13
3.1.1	Experimental setup	13
3.1.2	Results and discussion	17
3.2	Type-0 SPDC	19
3.2.1	Results and discussion	19
4	Conclusion	23
4.1	Outlook	24
A	Alignment procedure for optical setup	29

A narrowband photon pair source for quantum communication applications

Peh Yu Xiang

Engineering Science, Centre for Quantum Technologies, Singapore

Abstract—We propose and experimentally realize a highly non-degenerate spontaneous parametric down-conversion (SPDC) source of narrowband photon pairs, with the signal photons near the zero-dispersion wavelength of SMF-28e and in the sub-THz bandwidth regime. Attempts are made to produce this source using periodically-poled potassium titanyl phosphate (PPKTP) in Type-II SPDC with 401 nm pump beam and Type-0 SPDC with 405 nm pump beam. The generated signal photons have temperature-tunable wavelength of 1307.5 nm and frequency bandwidth of less than 0.1 nm, limited by spectrometer resolution. The low jitter of the source has promising applications in quantum communication requiring high time resolution.

Index Terms—Type-0 SPDC, PPKTP, narrowband, non-degenerate, telecommunication O-band

I. INTRODUCTION

The heart of quantum communication and computation involves detection and manipulation of light on the single photon level. Generation of a stream of single photons can be readily achieved through the use of a photon pair source that creates strongly time-correlated photon pairs. It is often desirable to reduce the bandwidth of the photons in the photon pair as well, e.g. in quantum key distribution (QKD), reducing the bandwidth of the coincidence window increases the signal-to-noise ratio and yields lower error rates.

The spontaneous parametric down-conversion (SPDC) optical process is commonly used to generate photon pairs, by pumping light into an optical medium that couples with the light in a non-linear manner. Owing to the weak coupling coefficient of such media, the natural bandwidth of the photon pairs generated is on the order of THz [1] [2] [3]. The bandwidth of the SPDC can even be reduced down to the MHz range through the use of cavities for spectral filtering. SPDC lends itself nicely to quantum communication applications since the frequency bandwidth of the photon output can be tuned to fall within the sub-THz regime using highly non-degenerate signal and idler photon wavelengths [4], without the use of additional optical elements or sensitive cavity alignment procedures.

A. Zero-dispersion wavelength

SPDC photon pair sources designed for quantum communication typically optimize for the C-band telecommunication band of optical fibers near 1550 nm where the lowest attenuation losses are exhibited [5] [4] [6] [7], to maximize brightness. However there exists a non-zero chromatic dispersion in the channel which introduces a wavelength-dependent change in transmission time. This broadening increases unwanted error rates during QKD, or timing uncertainty during clock synchronization, so dispersion must be corrected for by introducing additional dispersion compensation elements.

There exists a zero-dispersion wavelength in the O-band telecommunication channel at which we can generate the

photons using SPDC, typically at or near the 1310 nm wavelength for commercial telecommunication fibers. In addition, quantum communication protocols that utilize the 1310 nm frequency [8] can be also performed concurrently with simultaneous transmission of Internet data typically in the S-band (1460-1530 nm) and L-band (1565-1625 nm) [9] [10], with lower noise coupling. By generating signal photons at the zero-dispersion wavelength of SMF-28e with sub-THz bandwidth, the total timing jitter from SPDC and chromatic dispersion is on the order of sub-picoseconds, which is beyond the resolution limit of even the most state-of-the-art detectors. In other words, the resolution is not intrinsically limited by the source of photon pairs itself.

B. Narrowband non-degenerate SPDC

Existing work done to investigate non-degenerate SPDC have primarily focused on the production of narrowband photons near the 1550 nm wavelength. For example, König et al. [4] generated 1609 nm photons of 0.5 nm bandwidth using bulk periodically-poled lithium niobate (PPLN), while Kaneda et al. [7] produced 1590 nm photons with a bandwidth of about 1 nm using bulk PPKTP. Other works on non-degenerate SPDC to generate 1310 nm photons use cavity-enhanced SPDC to spectrally filter wavelengths to sub-GHz or MHz bandwidth regime instead [5] [11].

In this paper, we experimentally realize a non-degenerate SPDC photon pair source using a periodically-poled potassium titanyl phosphate (PPKTP) crystal. The signal output of this source is centered near 1310 nm with a narrow bandwidth of less than 0.1 nm, which can be temperature tuned to optimize for transmission at the zero-dispersion wavelength of SMF-28e optical fibers. Our proposed narrowband non-degenerate source for 1310 nm, to the best of our knowledge, has not yet been experimentally investigated.

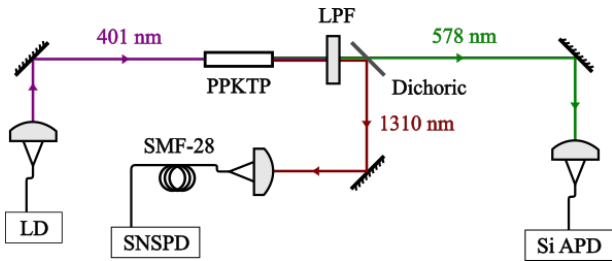
II. EXPERIMENTAL SETUP

A. Optical setup

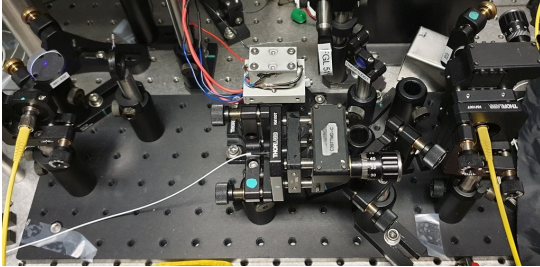
The optical setup for the down-conversion is shown in Figure 1a and Figure 1b.

The 401 nm pump beam is coupled into a single mode fiber with mode field diameter 2.0 — 2.4 μm at 350 nm (ThorLabs P1-305A-FC-1). With an aspheric lens of focal length 2.75 mm (ThorLabs C390TM-A), we create a 95 μm beam waist at a distance of 21 cm from the fiber where the PPKTP crystal is placed. The PPKTP crystal itself sits in an oven mounted on a manual rotation stage (ThorLabs PR01). A 3 mm thick longpass filter (Schott OG-530) with a transmittance of < -50 dB at 400 nm is placed close to the crystal to filter out the pump beam.

A shortpass dichroic mirror (DMSP1000T) separates the co-linear signal and idler photons. The near-infrared signal photons are coupled into a single mode SMF-28e fiber with



(a) Schematic of setup. LD: Pump laser diode; LPF Long-pass filter.



(b) Actual experimental optical setup

Fig. 1: The experimental setup using the PPKTP crystal for SPDC.

an aspheric lens of focal length 11 mm (ThorLabs C397TMD-C). The visible idler photons are coupled into a single mode fiber of mode field diameter around $4 \mu\text{m}$ at 488 nm with an aspheric lens of focal length 4.51 mm (ThorLabs C230TMD-A).

B. SPDC crystal

We use a periodically-poled potassium titanyl phosphate (PPKTP) crystal for non-degenerate narrowband photon pair generation. Two different SPDC processes were used in this paper: the type-II SPDC uses a 401 nm pump beam for $401 \text{ nm} (e) \rightarrow 1310 \text{ nm} (o) + 578 \text{ nm} (e)$ and a PPKTP crystal of a poling period of $\Lambda = 7.875 \mu\text{m}$ at room temperature fabricated by Raicol Crystals, while the type-0 SPDC uses a 405 nm pump beam for $405 \text{ nm} (o) \rightarrow 1310 \text{ nm} (o) + 586 \text{ nm} (o)$ and PPKTP crystal of poling period $\Lambda = 3.875 \mu\text{m}$. (e) and (o) represent the extraordinary and ordinary polarizations.

C. Laser source

For Type-II phase matching with 405 nm pump and 1310 nm signal photons, an high oven heating temperature of around 190°C is needed which is not ideal. The temperature requirement can be reduced to a more reasonable 40°C by replacing the 405 nm pump laser with a 401 nm pump laser. The Nichia NDV4316 laser diode is used to generate the pump beam, which has a center wavelength of approximately 401 nm and a multimode pump envelope. An external cavity diode laser (ECDL) setup in Littrow configuration is used to narrow the pump wavelength envelope, as shown in Figure 2.

Phase matching conditions for Type-0 SPDC with 405 nm pump are satisfied for a calculated oven temperature near 50°C . The single linewidth Ondax CP-405-PLR-40-4 laser diode is used, which has a specified center wavelength of $405 \pm 0.5 \text{ nm}$ and 160 MHz bandwidth using integrated volume Bragg grating.

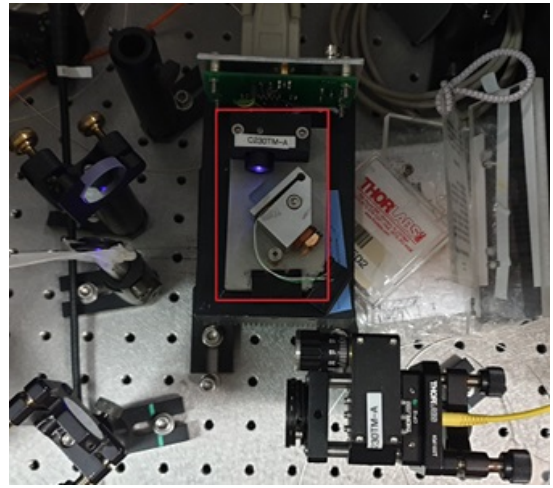


Fig. 2: Top-down view of the ECDL and coupling system. The ECDL in Littrow configuration is marked by the red rectangle.

D. Characterization devices

1) *Single photon detectors*: The total jitter from measuring cross-correlation between detection events is given by the convolution of all jitter contributions, including the intrinsic jitter of photon pair generation, temporal broadening from chromatic dispersion in the optical fiber, as well as the jitter of the single photon detectors.

The Si and InGaAs single photon avalanche photodetectors (APD) used in this paper are built in-house by the CQT Quantum Optics group. The Si APD used has a jitter of about 500 — 600 ps and a dark count rate of about 100 per second. The InGaAs APD used has a jitter of 200 — 300 ps and a dark count rate of about 10,000 per second.

Another single photon detector used is the superconducting nanowire single photon detector (SNSPD) which is a resonant structure comprising of nanometer-wide waveguides typically made from niobium nitride (NbN). It is designed for the near-infrared regime and has a negligible dark count rate of a few to around 100 accidentals per second. The jitter of the SNSPD used in this paper is around 40 ps.

2) *Spectrometers*: The wavelengths of single photons can be measured using grating spectrometry, which uses diffraction to select wavelengths for intensity measurement. The CDD-based grating spectrometer (OceanOptics USB2000+) is sensitive to light within the visible regime and has a wavelength resolution of 0.5 nm in this regime. We also use a rotating grating spectrometer in this paper borrowed from the NUS-Singtel Lab, is designed for the near-infrared regime with a wavelength resolution of about 1.0 nm.

III. RESULTS AND DISCUSSION

A. Type-II SPDC

The cross-correlation coincidence distribution obtained after Type-II SPDC is given in Figure 3. The jitter of the distribution is 600 ps, which is limited by the resolution of the detectors (specifically the Si APD). The signal photon spectrum is measured, as shown in Figure 4. Three prominent peaks at 1322 nm, 1334 nm, and 1349 nm can be seen, indicating that the signal spectrum is not single mode. This can be explained by the multimodal frequency distribution of the pump laser in the ECDL, which will not produce the

desired single mode down-conversion signal photons after Type-II SPDC.

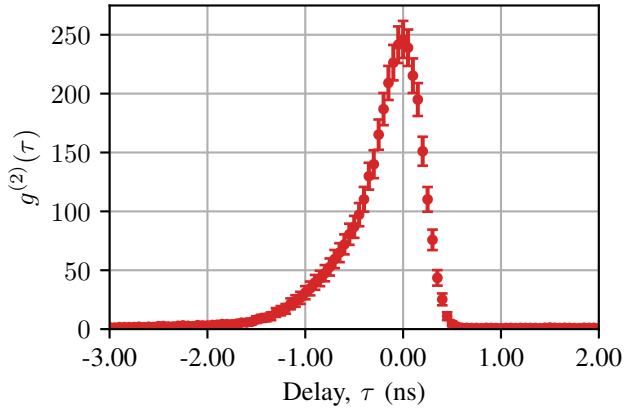


Fig. 3: Normalized cross-correlation between detection events on the SNSPD for the signal photons and Si APD for the idler photons, after Type-0 SPDC. The FWHM of the coincidence distribution is 600 ps.

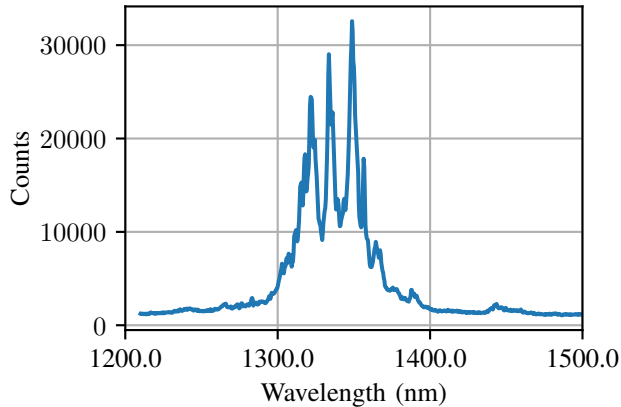


Fig. 4: Wavelength distribution of signal photons after Type-II SPDC with 401 nm pump beam from ECDL. The spectrum is clearly multimodal with multiple prominent peaks at 1322 nm, 1334 nm, and 1349 nm, as well as several other smaller peaks. The spectrometer resolution is 1.0 nm. Detection of photon arrival events is performed using SNSPD.

B. Type-0 SPDC

We turn to the 405 nm Ondax laser diode for Type-0 SPDC, which is measured to have center wavelength of 405.033 nm with a FWHM of 0.002 nm (frequency bandwidth of 3.7 GHz). The actual oven temperature after optimization for heralding efficiency is $38.7 \pm 0.1^\circ\text{C}$, with the heralding efficiency averaging around 8% obtained with the Type-0 SPDC. The $g^{(2)}$ cross-correlation has a jitter of 625 ps, as shown in Figure 5, which means the total jitter of the cross-correlation is still dominated by the jitter of the silicon APD.

The spectra of the signal and idler photons obtained is shown in Figure 6a and in Figure 6b, respectively. The measurements of bandwidth for both signal and idler are limited by the resolution of the respective spectrometer. The desired sub-THz bandwidth regime for the signal is achieved, since

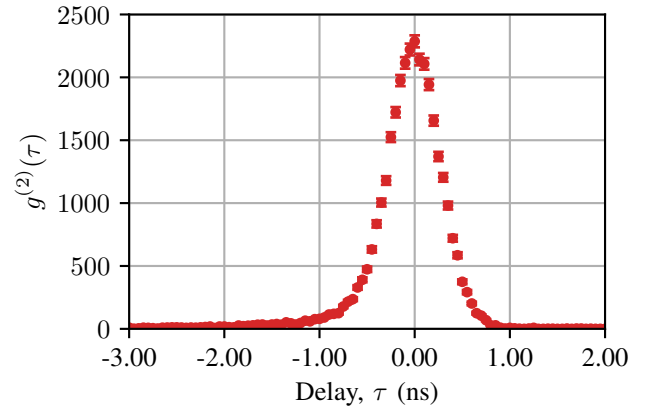


Fig. 5: Cross-correlation between detection events on the InGaAs APD for the signal photons and Si APD for the idler photons, after Type-0 SPDC. The FWHM of the coincidence distribution is 625 ps.

the 1.0 nm bandwidth (175 GHz frequency bandwidth) of the signal photon is an upper bound to the actual wavelength bandwidth of the signal.

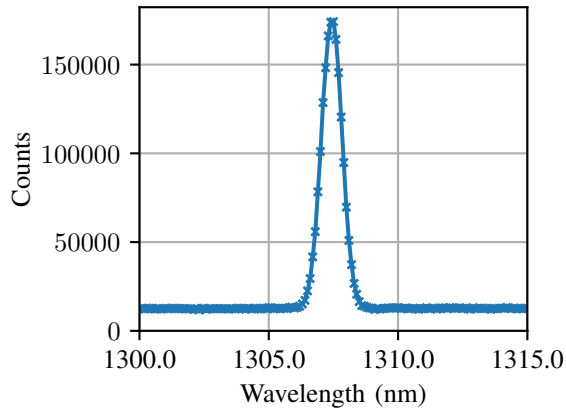
IV. CONCLUSION

We proposed a highly non-degenerate spontaneous parametric down-conversion (SPDC) source of narrowband photon pairs in the sub-THz bandwidth regime, and detailed the experimental setup necessary to facilitate the down-conversion of pump photons for both Type-II and Type-0 SPDC. The cross-correlation between the signal photon and idler photon detection events was measured to verify the presence of photon pairs.

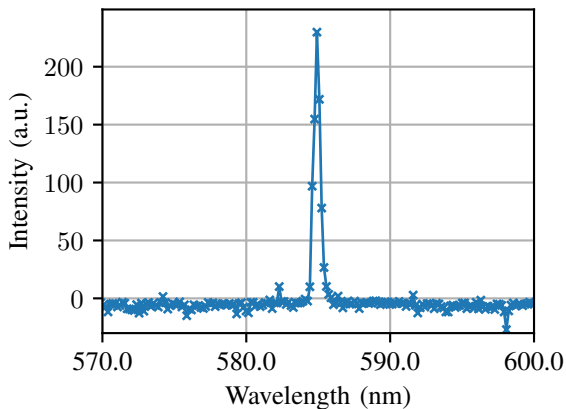
The 1.0 nm FWHM of the signal wavelength envelope indicates that our photon pair source is within the desired sub-THz bandwidth regime, despite being limited by the resolution of the spectrometers. The total jitter measured for a photon pair source in this sub-THz bandwidth regime, with the signal wavelength centered at the zero-dispersion wavelength of SMF-28e, is on the order of sub-picoseconds, which is very promising for high time resolution applications in quantum communication.

REFERENCES

- [1] P. G. Kwiat, K. Mattle, H. Weinfurter, A. Zeilinger, A. V. Sergienko, and Y. Shih. New high-intensity source of polarization-entangled photon pairs. *Phys. Rev. Lett.*, 75:4337–4341, Dec 1995.
- [2] P. G. Kwiat, E. Waks, A. G. White, I. Appelbaum, and P. H. Eberhard. Ultrabright source of polarization-entangled photons. *Phys. Rev. A*, 60:R773–R776, Aug 1999.
- [3] K. Hong, S. Baek, O. Kwon, and Y. Kim. Dispersive broadening of two-photon wave packets generated via type-i and type-ii spontaneous parametric down-conversion. *Journal of the Korean Physical Society*, 73:1650–1656, dec 2018.
- [4] F. König, E. J. Mason, F. N. C. Wong, and M. A. Albota. Efficient and spectrally bright source of polarization-entangled photons. *Phys. Rev. A*, 71:033805, Mar 2005.
- [5] J. Fekete, D. Rieländer, M. Cristiani, and H. de Riedmatten. Ultranarrow-band photon-pair source compatible with solid state quantum memories and telecommunication networks. *Phys. Rev. Lett.*, 110:220502, May 2013.
- [6] M. T. Liu and H. C. Lim. Transmission of o-band wavelength-division-multiplexed heralded photons over a noise-corrupted optical fiber channel. *Opt. Express*, 21(25):30358–30369, Dec 2013.
- [7] F. Kaneda, K. Garay-Palmett, A. B. U'Ren, and P. G. Kwiat. Heralded single-photon source utilizing highly nondegenerate, spectrally factorable spontaneous parametric downconversion. *Opt. Express*, 24(10):10733–10747, May 2016.



(a) Wavelength distribution of signal photons centered at 1307.5 nm with a FWHM of approximately 1.0 nm. The rotating grating spectrometer of resolution 1.0 nm is used, and the photon detection counts are measured using the InGaAs APD.



(b) Wavelength distribution of idler photons centered at 584.9 nm with a FWHM of approximately 0.6 nm, measured using the OceanOptics spectrometer of resolution 0.5 nm.

Fig. 6: Wavelength distribution of signal and idler photons after the Type-0 SPDC using 405 nm pump laser. Both spectra are limited by the resolution of the spectrometers.

- [8] J. Lee, L. Shen, A. N. Utama, and C. Kurtsiefer. Absolute clock synchronization with a single time-correlated photon pair source over 10km. 2020.
- [9] N. I. Nweke, P. Toliver, R. J. Runser, S. R. McNown, J. B. Khurgin, T. E. Chapuran, M. S. Goodman, R. J. Hughes, C. G. Peterson, K. McCabe, J. E. Nordholt, K. Tyagi, P. Hiskett, and N. Dallmann. Experimental characterization of the separation between wavelength-multiplexed quantum and classical communication channels. *Applied Physics Letters*, 87(17):174103, 2005.
- [10] T. E. Chapuran, P. Toliver, N. A. Peters, J. Jackel, M. S. Goodman, R. J. Runser, S. R. McNown, N. Dallmann, R. J. Hughes, K. P. McCabe, J. E. Nordholt, C. G. Peterson, K. T. Tyagi, L. Mercer, and H. Dardy. Optical networking for quantum key distribution and quantum communications. *New Journal of Physics*, 11(10):105001, oct 2009.
- [11] C. Clausen, F. Bussières, A. Tiranov, H. Herrmann, C. Silberhorn, W. Sohler, M. Afzelius, and N. Gisin. A source of polarization-entangled photon pairs interfacing quantum memories with telecom photons. *New Journal of Physics*, 16(9):093058, sep 2014.

List of Figures

1.1	Cross-correlation between detection events on separate photon detectors, where the red area is background noise and green area is the coincidence signal. The green area is the same across (a) and (b). Narrower bandwidth photons manifest as a sharper peak during detection in (a) as compared to (b). Integrating over a smaller coincidence window yields a larger signal-to-noise ratio.	2
1.2	Plot of dispersion per kilometer of Corning SMF-28e optical fiber as a function of wavelength. The zero-dispersion wavelength for this fiber is 1313 nm. The total dispersion can be obtained by integrating the dispersion curve over the wavelength bandwidth.	3
2.1	Plot of the sinc squared function. Note that the zeroes of the function occurs at integer multiples of π	7
2.2	Refractive index of birefringent KTP crystal as a function of wavelength of light with ordinary and extraordinary polarization, at room temperature. These curves are obtained using the experimentally-fitted temperature-dependent Sellmeier equations. The crystal exhibits normal dispersion for each polarization.	7
2.3	Plot of wavevector mismatch against signal wavelength for pump beam of 405 nm, in room temperature PPKTP for Type-0 SPDC. The photon polarizations all share the same polarization as the ordinary ray.	9
2.4	Si APD built in-house by the CQT Quantum Optics group.	11
2.5	SNSPD mounted on the 4K cooling stage of a cryogenic fridge. The SNSPDs are circled in white.	12
2.6	False-color scanning electron micrograph of a sample SNSPD structure. Image provided by NIST.	12
3.1	Damage to the wire jackets from heating the oven holder to 190°C.	14
3.2	The experimental setup using the PPKTP crystal for SPDC.	14

3.3	Top-down view of the ECDL and coupling system. The ECDL in Littrow configuration is marked by the red rectangle.	16
3.4	Wavelength spectrum of pump laser diode in ECDL setup, obtained using OceanOptics spectrometer. The center wavelength is 400.5 nm with a wavelength envelope FWHM of 0.5 nm.	16
3.5	Normalized cross-correlation between detection events on the SNSPD for the signal photons and Si APD for the idler photons, after Type-0 SPDC. The FWHM of the coincidence distribution is 600 ps.	17
3.6	Wavelength distribution of signal photons after Type-II SPDC with 401 nm pump beam from ECDL. The spectrum is clearly multimodal with multiple prominent peaks at 1322 nm, 1334 nm, and 1349 nm, as well as several other smaller peaks. The spectrometer resolution is 1.0 nm. Detection of photon arrival events is performed using SNSPD.	18
3.7	Spectrum of pump laser ECDL measured using spectrometer of resolution of < 1.0 parts per million. The spectrum is multimode with a peak center wavelength of 400.407 nm.	18
3.8	Cross-correlation between detection events on the InGaAs APD for the signal photons and Si APD for the idler photons, after Type-0 SPDC. The FWHM of the coincidence distribution is 625 ps.	20
3.9	Spectrum of narrow bandwidth laser diode (Ondax CP-405-PLR-40-4) at a supplied laser current of 72.5 mA. The center wavelength is 405.033 nm with a FWHM of 0.002 nm.	20
3.10	Wavelength distribution of signal and idler photons after the Type-0 SPDC using 405 nm pump laser. Both spectra are limited by the resolution of the spectrometers.	21

Chapter 1

Introduction

1.1 Narrowband photon pair source

The heart of quantum communication and computation involves detection and manipulation of light on the single photon level. Generation of a stream of single photons can be readily achieved through the use of a photon pair source that creates strongly time-correlated photon pairs, i.e., the detection of one of the photons in the pair can be used to signal the presence of the other photon.

It is often desirable to reduce the bandwidth of the photons in the photon pair as well. In quantum key distribution (QKD), reducing the bandwidth of the coincidence window increases the signal-to-noise ratio, as shown in Figure 1.1, which yields lower error rates. Extremely narrow photons on the order of MHz can even be used to interface with atoms with narrow atomic transitions and quantum memory [1][2].

1.2 SPDC for quantum communication

The spontaneous parametric down-conversion (SPDC) optical process is commonly used to generate photon pairs. These photon pairs are obtained by pumping light into an optical medium, such as potassium titanyl phosphate (KTP) and barium borate (BBO), that couples with the light in a non-linear manner. Owing to the weak coupling coefficient of such media, the natural bandwidth of photon pairs is on the order of THz [3][4][5]. The bandwidth of the SPDC can be reduced down to the MHz range through the use of cavities for spectral filtering, such as the bow-tie configuration [6][7], Fabry-Perot [2][8], or even the crystal itself as a cavity mirror [9].

Notably, SPDC lends itself nicely to quantum communication applications since the frequency bandwidth of the photon output can be tuned to fall within the sub-

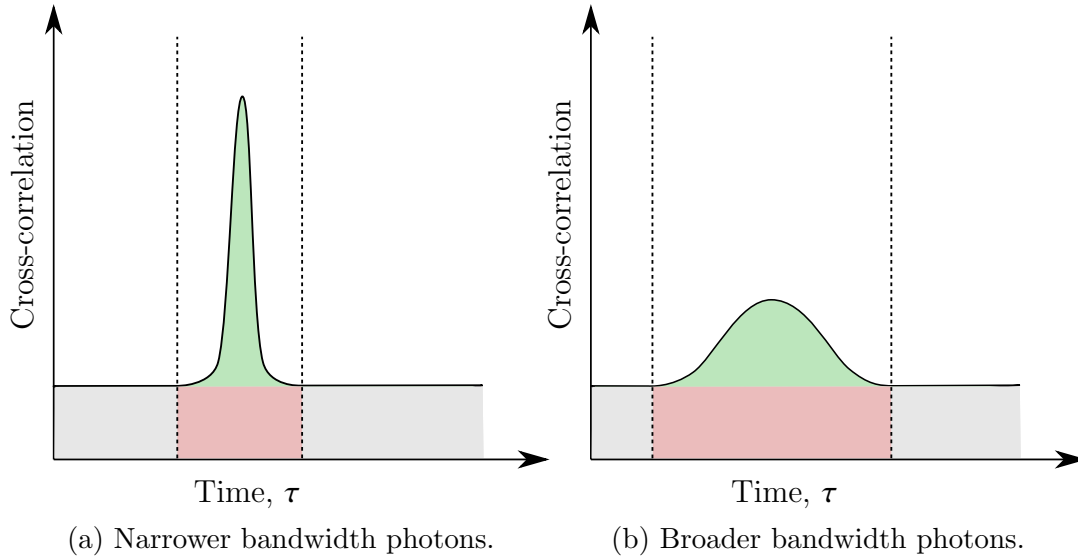


Figure 1.1: Cross-correlation between detection events on separate photon detectors, where the red area is background noise and green area is the coincidence signal. The green area is the same across (a) and (b). Narrower bandwidth photons manifest as a sharper peak during detection in (a) as compared to (b). Integrating over a smaller coincidence window yields a larger signal-to-noise ratio.

THz regime using highly non-degenerate signal and idler photon wavelengths [10], without the use of additional optical elements or sensitive cavity alignment procedures. The physical explanation for this phenomena is detailed in Chapter 2 of the thesis.

SPDC photon pair sources designed for quantum communication typically optimize for the C-band telecommunication band of optical fibers near 1550 nm where the lowest attenuation losses are exhibited [1][10][11][12], to maximize the brightness. However there exists a non-zero chromatic dispersion in the channel which introduces a wavelength-dependent change in transmission time, as shown in Figure 1.2 (the dispersion equation is supplied by the manufacturer [13]). This arises from the fact that the refractive index of the fiber (and hence speed of light in the fiber) varies with the wavelength of the propagating light. This broadening increases unwanted error rates during QKD, or timing uncertainty during clock synchronization, so dispersion must be corrected for by introducing additional dispersion compensation elements.

There exists a zero-dispersion wavelength in the O-band telecommunication channel at which we can generate the photons using SPDC, typically at or near the 1310 nm wavelength for commercial telecommunication fibers as seen in Figure 1.2. In addition, quantum communication protocols that utilize the 1310 nm frequency [14] can be also performed concurrently with simultaneous transmission of Internet data typically in the S-band (1460-1530 nm) and L-band (1565-1625

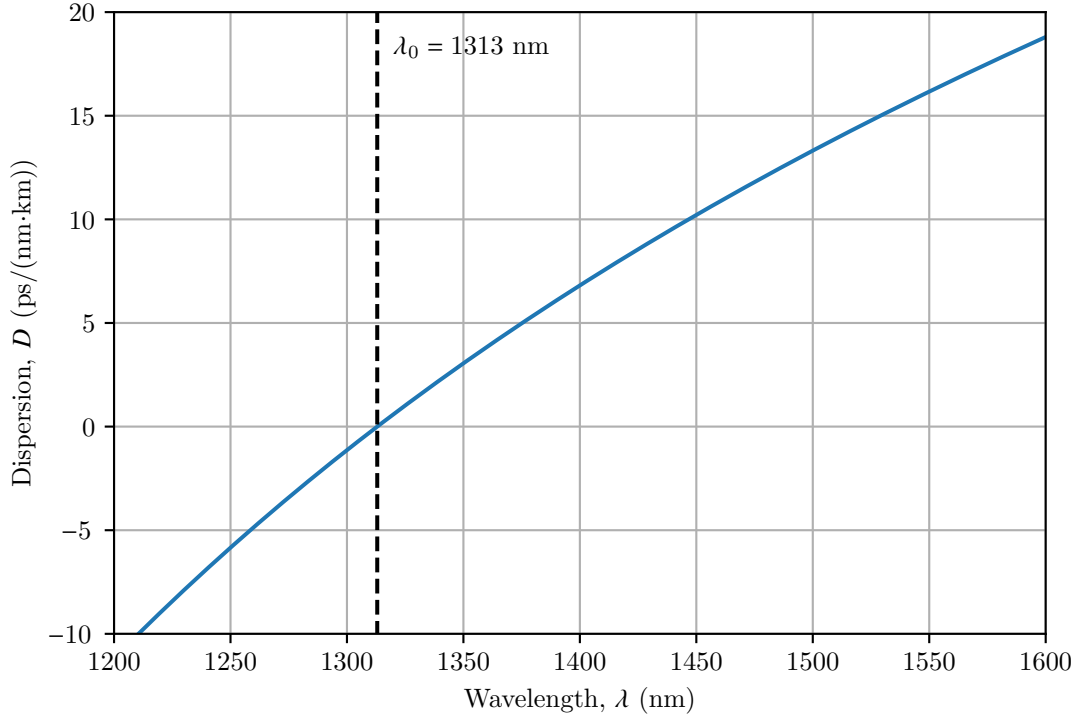


Figure 1.2: Plot of dispersion per kilometer of Corning SMF-28e optical fiber as a function of wavelength. The zero-dispersion wavelength for this fiber is 1313 nm. The total dispersion can be obtained by integrating the dispersion curve over the wavelength bandwidth.

nm) [15][16], with lower noise coupling by virtue of the larger wavelength separation compared to C-band (1530-1565 nm) wavelengths.

We can show that the sub-THz regime of the SPDC output bandwidth is suitable for quantum communication. Suppose we generate a signal photon centered at 1313 nm with wavelength bandwidth of 1 nm, corresponding to a frequency bandwidth of 174 GHz. Note that due to the uncertainty principle, there is an intrinsic lower bound to the timing uncertainty between photon pairs during down-conversion, given by $\Delta t \geq \frac{\hbar}{2\Delta E} = \frac{1}{4\pi\Delta f} = 0.5$ ps. The dispersion of these photons in a 10-km long optical fiber is approximately 0.2 ps using Figure 1.2. The total timing jitter is thus on the order of sub-picoseconds, which is beyond the resolution limit of even the most state-of-the-art detectors today, i.e. the resolution is not intrinsically limited by the source of photon pairs itself. The use of non-degenerate SPDC also allows the idler photon in the visible wavelength regime to be detected by higher efficiency silicon photodetectors, increasing the heralding efficiency of the down-conversion.

1.3 Outline of thesis

In this thesis, we experimentally realize a non-degenerate SPDC photon pair source using a periodically-poled potassium titanyl phosphate (PPKTP) crystal. The signal output of this source is centered near 1310 nm with a narrow bandwidth of less than 0.1 nm, which can be temperature tuned to optimize for transmission at the zero-dispersion wavelength of SMF-28e optical fibers.

Existing work done to investigate non-degenerate SPDC have primarily focused on the production of narrowband photons near the 1550 nm wavelength. For example, König et al. [10] generated 1609 nm photons of 0.5 nm bandwidth using bulk periodically-poled lithium niobate (PPLN), while Kaneda et al. [12] produced 1590 nm photons with a bandwidth of about 1 nm using bulk PPKTP. Other works on non-degenerate SPDC to generate 1310 nm photons use cavity-enhanced SPDC to spectrally filter wavelengths to sub-GHz or MHz bandwidth regime instead [1][2]. Our proposed narrowband non-degenerate source for 1310 nm, to the best of our knowledge, has not yet been experimentally investigated.

The theory behind SPDC is detailed in Chapter 2 of the thesis, as well as the equipment used to characterize the generated photon pairs. The experimental setup and the results are described in Chapter 3. We finally conclude the thesis in Chapter 4 and explore possible avenues for extending this work.

Chapter 2

Preliminaries

2.1 Spontaneous parametric down-conversion

2.1.1 Heralded photon source

Spontaneous parametric down-conversion (SPDC) is a non-linear optical process used to create photon pairs that are strongly time-correlated. Photons in the pump laser beam are converted into pairs of downstream photons, termed as the signal and idler photons, as they propagate through a crystal. This process manifests as a result of the non-linearity of the crystal's electric susceptibility χ under strong electric fields, expressed as a power series in the electric field strength E ,

$$P = \varepsilon_0 \left[\chi^{(1)} E + \chi^{(2)} E^2 + \dots \right] \quad (2.1)$$

where the polarization P is a function of the familiar linear susceptibility $\chi^{(1)}$ and the (second) higher-order non-linear susceptibility $\chi^{(2)}$ [17]. SPDC itself is a second-order non-linear process that depends on $\chi^{(2)}$.

Photons generated by SPDC in the non-linear crystal must be generated as a pair, with a timing separation typically within sub-picoseconds of each other. The detection of one photon from a pair thus indicates the existence of the other photon in the pair — in other words, the detected photon *heralds* the other photon. This also means that when both photons are detected, there exists some time difference τ between the two detection events. The pairwise detection event is termed as a *coincidence event*.

A related concept is the heralding efficiency η , defined as the ratio of photon pair detection events P to the geometric mean of single photon detection events on both detectors S_1 and S_2 , within this coincidence window,

$$\eta = \frac{P}{\sqrt{S_1 \times S_2}}. \quad (2.2)$$

2.1.2 Phase matching

The generation of photon pairs during SPDC is maximized when the *phase matching* conditions are met, i.e., the set of energy and momentum conservation conditions,

$$E_p - E_i - E_s = 0 \quad (2.3)$$

$$\Delta k = k_p - k_i - k_s = 0 \quad (2.4)$$

are fulfilled between the pump p , idler i and signal s photons. $E = hf = hc/\lambda$ is the energy of the photon, while $k = 2\pi n/\lambda$ is the wavevector of the photon. Note that k is related to the wavelength-dependent refractive index of the medium $n(\lambda)$. The direction-dependence of the wavevector is removed by assuming the phase propagation direction of the pump, signal and idler photons are all co-linear, which is true for the SPDC process used in this thesis. The wavevector mismatch Δk thus represents the relative phase propagation between that of the signal and idler fields along the same direction.

The classical picture of SPDC is best used to explain how momentum conservation can be satisfied. By using the coupled-wave equations of the SPDC and modelling the output fields as plane waves, the intensity I of the output waves can be expressed as a function of Δk ,

$$I = I^{(\max)} \operatorname{sinc}^2 \left(\frac{\Delta k L}{2} \right) \quad (2.5)$$

where L is the length of the crystal used in the SPDC process. The plot of the squared sinc function is as shown in Figure 2.1. The full treatment of the SPDC process in both the classical and quantum picture is beyond the scope of this thesis, but can be found in many reference texts [17][18][19].

We observe that the wavevector mismatch Δk ideally should be as close to 0 as possible for maximum brightness. It has been shown that *perfect phase matching*, specifically when $\Delta k = 0$, cannot be achieved with a single polarization in the normal dispersion region of a medium [18], where the refractive index decreases monotonically with increasing wavelength λ . Figure 2.2 illustrates this particular

2.1. Spontaneous parametric down-conversion

refractive index behaviour for the potassium titanyl phosphate (KTP) crystal at room temperature, plotted using the Sellmeier equations [20][21][22].

Birefringence of the crystal can be used to compensate for the wavevector mismatch Δk , as the refractive index differs between light of different polarizations. Temperature can be used to further tune the refractive index of the crystal.

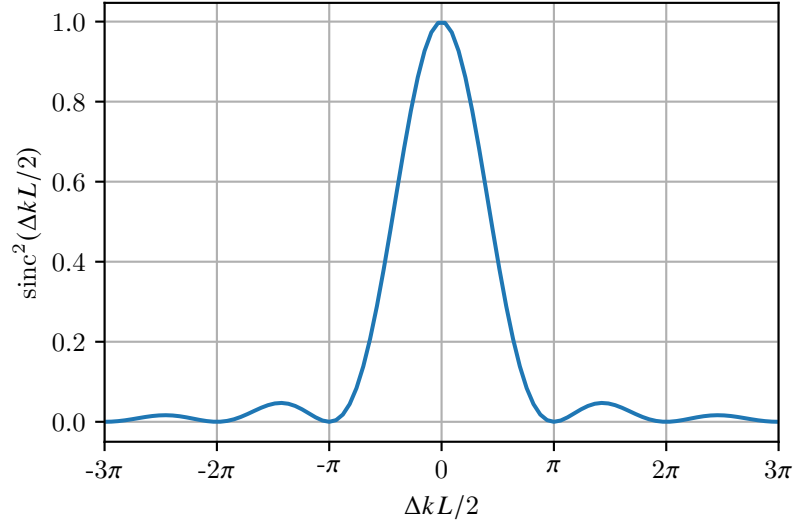


Figure 2.1: Plot of the sinc squared function. Note that the zeroes of the function occurs at integer multiples of π .

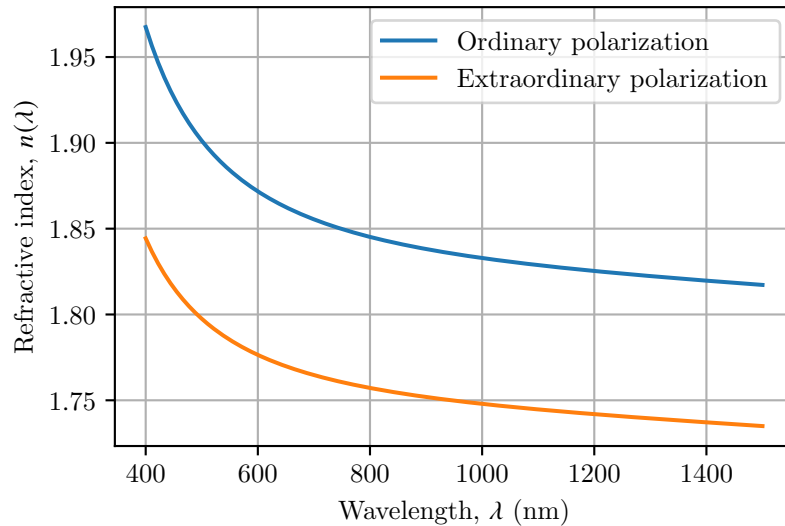


Figure 2.2: Refractive index of birefringent KTP crystal as a function of wavelength of light with ordinary and extraordinary polarization, at room temperature. These curves are obtained using the experimentally-fitted temperature-dependent Sellmeier equations. The crystal exhibits normal dispersion for each polarization.

2.1.3 Quasi-phase matching

There are cases where birefringence is still insufficient to compensate for the wavevector mismatch Δk .

A non-zero Δk results in a phase difference between the pump and output fields that accumulates throughout the length L of the crystal. While the fields are in-phase, energy couples from the pump field into the output field. Correspondingly, the energy in the output field couples back into the pump field when the fields are out-of-phase, resulting in a decrease in output intensity.

A technique known as *periodic poling* can be used to keep the fields in-phase. When the pump and output waves accumulate a π phase difference, the parity of the crystal coupling coefficient can be changed by flipping the ferroelectric domains of the crystal, thereby reversing the phase difference. This allows energy from the pump field to continue coupling into the output field.

The periodic flipping of the ferroelectric domains with every 2π phase accumulation across a periodic poling length of Λ contributes an additional momentum term that compensates for the wavevector mismatch,

$$\Delta k = k_p - k_i - k_s - \frac{2\pi}{\Lambda} = 0. \quad (2.6)$$

The poling period of the crystal for a desired down-conversion process can thus be specified, accounting for the temperature T and wavelength λ dependence of the refractive index as well as the linear thermal expansion coefficient α_L of the crystal,

$$\Lambda(\lambda, T) = \frac{2\pi(1 + \alpha_L(T - 25))}{k_p(\lambda_p, T) - k_s(\lambda_s, T) - k_i(\lambda_i, T)}. \quad (2.7)$$

The use of periodically-poled crystals, such as periodically-poled potassium titanyl phosphate (PPKTP), is often a desirable approach since crystals of different periodicity can be engineered to compensate for a wide range of wavevector mismatches, as well as allow for co-linear operation.

SPDC can be subclassified by the orthogonality of polarization between the pump, idler and signal photons. By convention, Type-0 SPDC denotes the use of the same polarization across all three photons, Type-I SPDC denote orthogonal polarizations between the signal + idler photons and the pump photon, while Type-II SPDC denote orthogonal polarizations between the signal and idler photon.

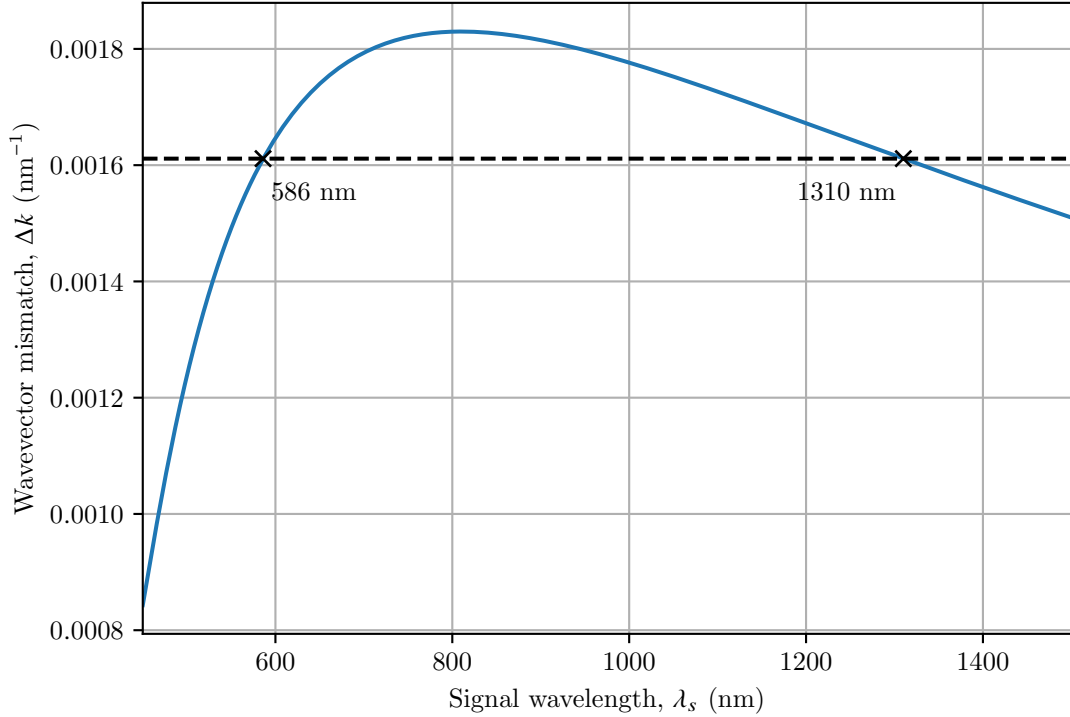


Figure 2.3: Plot of wavevector mismatch against signal wavelength for pump beam of 405 nm, in room temperature PPKTP for Type-0 SPDC. The photon polarizations all share the same polarization as the ordinary ray.

2.1.4 Non-degenerate photon pairs

In Chapter 1, we briefly mentioned that the use of non-degenerate signal and idler photon wavelengths can lead to a significant reduction in frequency bandwidth. This is best illustrated graphically, with Figure 2.3 showing a plot of wavevector mismatch $\Delta k = k_p - k_i - k_s$ against wavelength of the signal photon λ_s for a pump beam of $\lambda_p = 405$ nm and PPKTP at room temperature. The polarizations of photons are assumed to be in the same polarization (Type-0 SPDC) to aid in conceptual understanding.

There are three notable features in the graph:

1. The wavevector mismatch Δk is never equal to zero within the normal dispersion regime.
2. The maximum value of Δk occurs when the photon pairs are degenerate, i.e. $\lambda_s = \lambda_i = 810$ nm.
3. The points where the horizontal line intersect indicate the wavelengths for which energy is conserved, e.g. 405 nm \rightarrow 1310 nm + 586 nm.

For a given compensation of Δk during quasi-phase matching, we obtain the

wavelengths for which phase matching conditions are met. Near the degenerate wavelength $\lambda_s = \lambda_i = 810$ nm, a small deviation in Δk results in a relatively wide bandwidth shift. This contrasts to when $\lambda_s = 1310$ nm, where a small Δk deviation results in a relatively smaller change in bandwidth for the signal photon and correspondingly for the idler. The use of non-degenerate photon pair generation during SPDC decreases the wavelength bandwidth of photons in the pair.

2.2 Detection of photon pairs

2.2.1 Single photon detection

The total jitter from measuring cross-correlation between detection events is given by the convolution of all jitter contributions, including the intrinsic jitter of photon pair generation, temporal broadening from chromatic dispersion in the optical fiber, as well as the jitter of the single photon detectors. It is thus important to understand the characteristics of the detectors used to measure the $g^{(2)}$ cross-correlation.

Avalanche photodetectors

Single photon avalanche photodetectors (APD) rely on the avalanche effect to generate a signal pulse of significantly higher energy than that of a single photon.

Typical APDs maintain a large reverse bias voltage across a semiconductor PN junction that exceeds the breakdown voltage. This metastable state is so sensitive that the absorption of a single photon within the depletion region is sufficient to trigger the multiplication of charge carriers that generate the avalanche current. APDs are usually cooled to low temperatures to minimize thermal fluctuations contributing to dark counts in the detectors.

The responsivity of APDs is wavelength-dependent, depending on the semiconductor stack used. Silicon (Si) avalanche detectors have high detection efficiencies across the entire visible spectrum, while indium-gallium-arsenide (InGaAs) avalanche detectors are sensitive in the near-infrared regime.

The Si and InGaAs APDs used in this thesis are built in-house by the CQT Quantum Optics group. Figure 2.4 shows the Si APD. The Si APD used has a jitter of about 500 — 600 ps and a dark count rate of about 100 per second. The InGaAs APD used has a jitter of 200 — 300 ps and a dark count rate of about 10,000 per second. Note that the dark count rate of APDs is strongly correlated to the operating conditions.

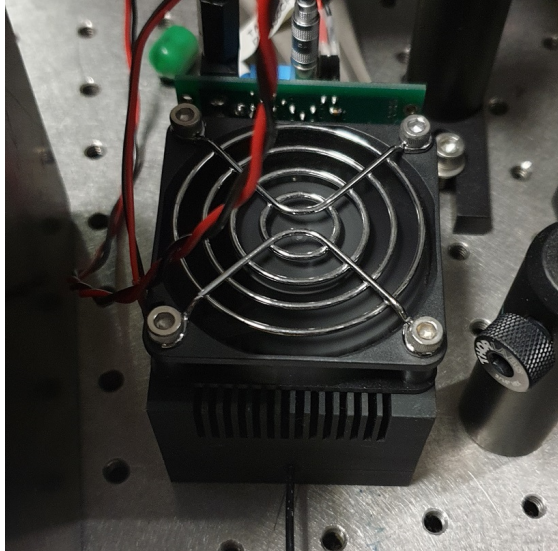


Figure 2.4: Si APD built in-house by the CQT Quantum Optics group.

Superconducting nanowire

The superconducting nanowire single photon detector (SNSPD) is a resonant structure comprising of nanometer-wide waveguides, typically made from niobium nitride (NbN). Figure 2.6 shows one such example of a nanostructure fabricated for use as an SNSPD, provided by the USA National Institute of Standards and Technology (NIST).

The SNSPD is kept in the superconducting state by cooling, and a bias current just under the critical current is supplied across the SNSPD. The detection of single photons in the SNSPD can be understood as the formation of a local hotspot within the nanostructure upon absorption of a photon, causing the region to briefly become non-superconducting and reflect the bias current into the output as a signal pulse. The region subsequently cools and returns to the superconducting state for the next photon detection.

While the SNSPD can be engineered to become sensitive to a wide variety of wavelengths, the efficiency of SNSPD is typically enhanced for a specified wavelength through the use of resonant nanostructures and distributed Bragg gratings.

The SNSPD used in the thesis is housed within the 4K cooling stage of a cryogenic fridge supplied by Entropy Cryogenics, as shown in Figure 2.5. It is designed for the near-infrared regime and has a negligible dark count rate of a few to around 100 accidentals per second. The jitter of the SNSPD used in this thesis is around 40 ps. This jitter can be reduced using cryogenic electronics and related work is still ongoing.

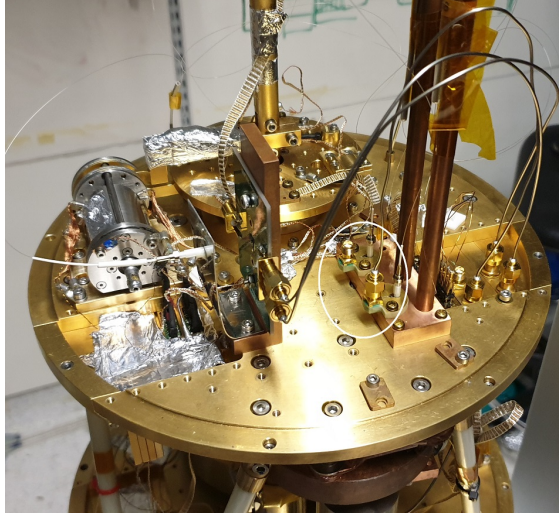


Figure 2.5: SNSPD mounted on the 4K cooling stage of a cryogenic fridge. The SNSPDs are circled in white.

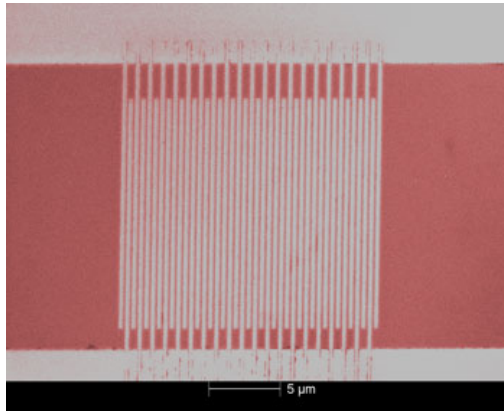


Figure 2.6: False-color scanning electron micrograph of a sample SNSPD structure. Image provided by NIST.

2.2.2 Spectral bandwidth measurement

The wavelengths of single photons can be measured using grating spectrometry, which uses diffraction to select wavelengths for intensity measurement.

The CDD-based grating spectrometer typically has a fixed diffraction grating which diffracts light into the pixels of a linear CCD camera. The OceanOptics spectrometer (OceanOptics USB2000+) used in this thesis is based on this design. It is sensitive to light within the visible regime and has a wavelength resolution of 0.5 nm in this regime.

A reflective grating can also be mounted onto a rotation stage that diffracts light according to the grating equation. The diffracted light is then coupled into a single mode fiber for subsequent detection by a single photon detector. The grating spectrometer used in this thesis was borrowed from the NUS-Singtel Lab and is designed for the near-infrared regime, with a wavelength resolution of 1.0 nm.

Chapter 3

Experimental results

3.1 Type-II SPDC

In this chapter, we explore the use of a periodically-poled potassium titanyl phosphate (PPKTP) crystal for non-degenerate narrowband photon pair generation. The PPKTP crystal is fabricated by Raicol Crystals with a poling period of $\Lambda = 7.875 \mu\text{m}$ at room temperature.

The PPKTP poling period for Type-II SPDC with 405 nm pump and 1310 nm signal photons is $8.27 \mu\text{m}$ at room temperature, as calculated with Equation 2.7. An oven heating temperature of around 190°C is needed to achieve phase matching, which is not ideal due to the fire hazard: the wire jacket and solder can potentially melt at the high temperature, shown in Figure 3.1, and fluctuations at high temperatures can risk damaging the crystal. A large heating current also has to be continuously drawn to maintain the temperature.

The temperature requirement can be reduced to a more reasonable 40°C by replacing the 405 nm pump laser with a 401 nm pump laser. This gives the following down-conversion process:

$$401 \text{ nm (e)} \rightarrow 1310 \text{ nm (o)} + 578 \text{ nm (e)}$$

where (e) and (o) represent the extraordinary and ordinary polarizations.

3.1.1 Experimental setup

Optical setup

The optical setup for the down-conversion is shown in Figure 3.2a and Figure 3.2b.

The 401 nm pump beam is coupled into a single mode fiber with mode field diameter $2.0 - 2.4 \mu\text{m}$ at 350 nm (ThorLabs P1-305A-FC-1). With an aspheric lens of focal length 2.75 mm (ThorLabs C390TM-A), we create a $95 \mu\text{m}$ beam

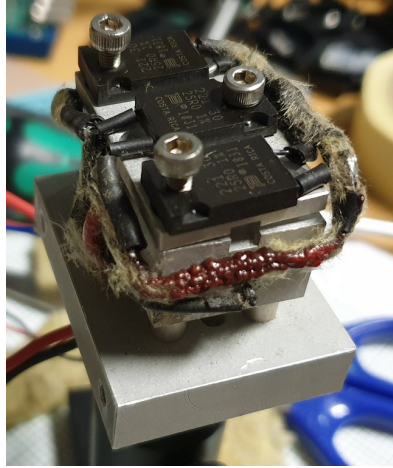
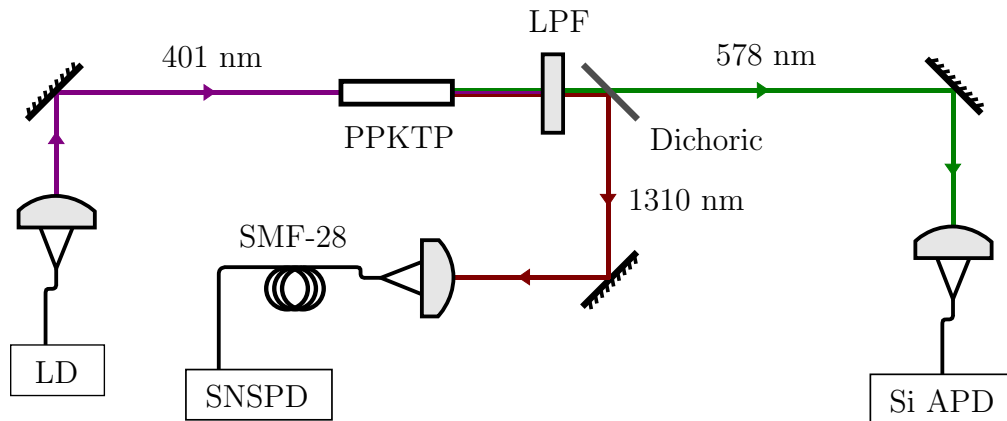
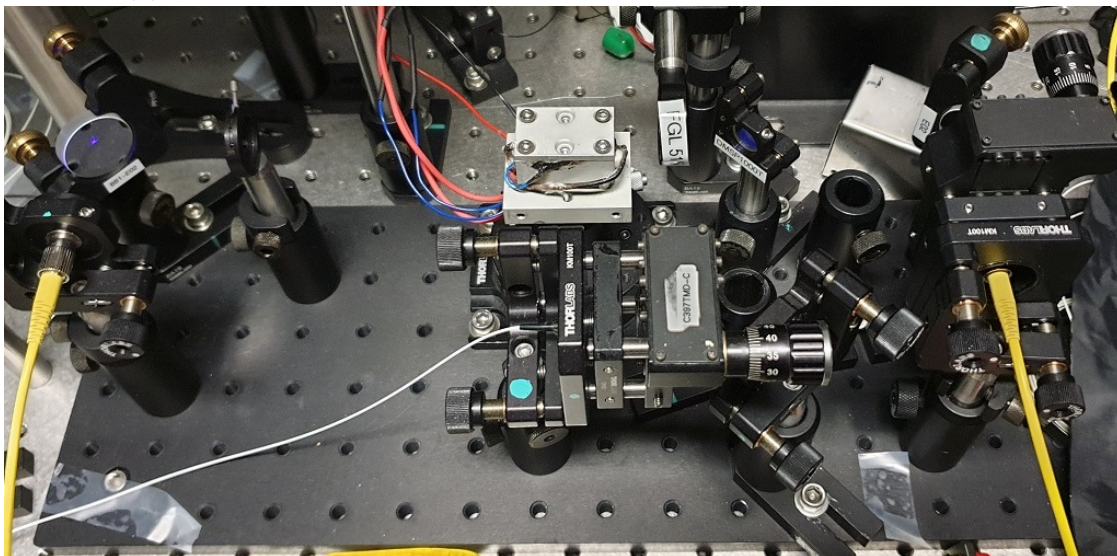


Figure 3.1: Damage to the wire jackets from heating the oven holder to 190°C.



(a) Schematic of setup. LD: Pump laser diode; LPF Long-pass filter.



(b) Actual experimental optical setup

Figure 3.2: The experimental setup using the PPKTP crystal for SPDC.

waist at a distance of 21 cm from the fiber where the PPKTP crystal is placed. The pump beam waist is chosen using the Bennink model [23][24], by optimizing for heralding efficiency assuming no collection and detector loss. The PPKTP crystal itself sits in an oven mounted on a manual rotation stage (ThorLabs PR01). A 3 mm thick longpass filter (Schott OG-530) with a transmittance of < -50 dB at 400 nm is placed close to the crystal to filter out the pump beam.

A shortpass dichoric mirror (DMSP1000T) separates the co-linear signal and idler photons. The near-infrared signal photons are coupled into a single mode SMF-28e fiber with an aspheric lens of focal length 11 mm (ThorLabs C397TMD-C). The visible idler photons are coupled into a single mode fiber of mode field diameter around 4 μm at 488 nm with an aspheric lens of focal length 4.51 mm (ThorLabs C230TMD-A).

Coincidence measurement

The idler photons are coupled into the Si avalanche photodetector, while the signal photons are coupled into the SNSPD. The signal output from the detectors are converted into nim pulses using discriminator cards and fed into a timestamp card for cross-correlation between photon detection events to identify the coincidence peak.

Laser source

The Nichia NDV4316 laser diode is used to generate the pump beam, which has a center wavelength of approximately 401 nm and a multimode pump envelope. An external cavity diode laser (ECDL) setup in Littrow configuration is used to narrow the pump wavelength envelope, as shown in Figure 3.3. This setup is achieved through the use of a 3600 lines/mm reflective grating (ThorLabs GH25-36U) that reflects the desired 401 nm wavelength as a feedback to the laser diode, forming an external cavity between the grating and the diode. The alignment procedure for the ECDL is referenced from MacAdam et al. [25].

The pump wavelength spectrum is initially characterized using the OceanOptics spectrometer, as shown in Figure 3.4.

Crystal oven holder

The PPKTP crystal is housed within the aluminium oven, shown in Figure 3.2b, which has a 5 Ω heating resistor and PID controller to stabilize the temperature at around 40.0°C with fluctuations of less than 0.1°C. The heat loss from the oven is further minimized by capping the oven with a thin aluminium housing to reflect radiation and provide an insulating air layer.

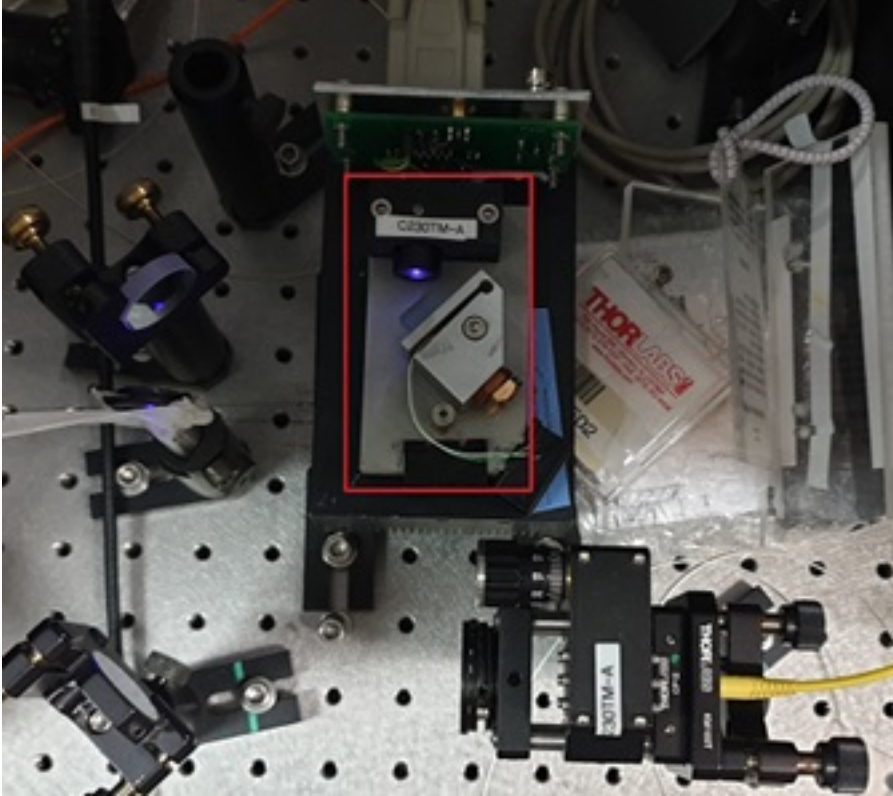


Figure 3.3: Top-down view of the ECDL and coupling system. The ECDL in Littrow configuration is marked by the red rectangle.

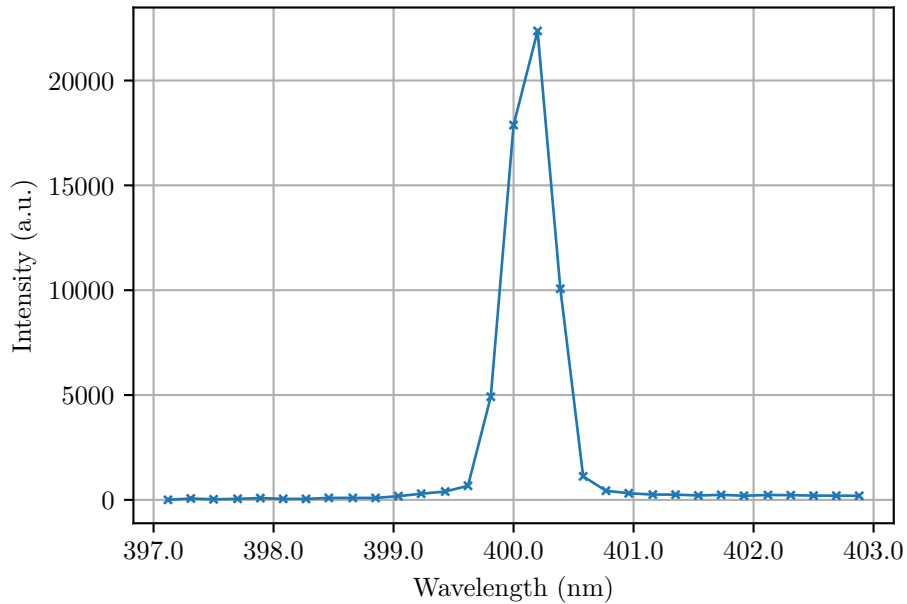


Figure 3.4: Wavelength spectrum of pump laser diode in ECDL setup, obtained using OceanOptics spectrometer. The center wavelength is 400.5 nm with a wavelength envelope FWHM of 0.5 nm.

3.1.2 Results and discussion

The cross-correlation coincidence distribution obtained after Type-II SPDC is given in Figure 3.5. The jitter of the distribution is 600 ps, which is limited by the resolution of the detectors (specifically the Si APD).

The signal photon spectrum is measured, as shown in Figure 3.6. Three prominent peaks at 1322 nm, 1334 nm, and 1349 nm can be seen, indicating that the signal spectrum is not single mode.

A Michelson interferometric spectrometer with resolution at least 1.0 parts per million (Bristol Model 771) is used to characterize the pump wavelength spectrum to a higher accuracy than is afforded by the OceanOptics spectrometer, as shown in Figure 3.7. The pump laser still has a multimodal frequency distribution in external cavity configuration which will not produce the desired single mode down-conversion signal photons after SPDC.

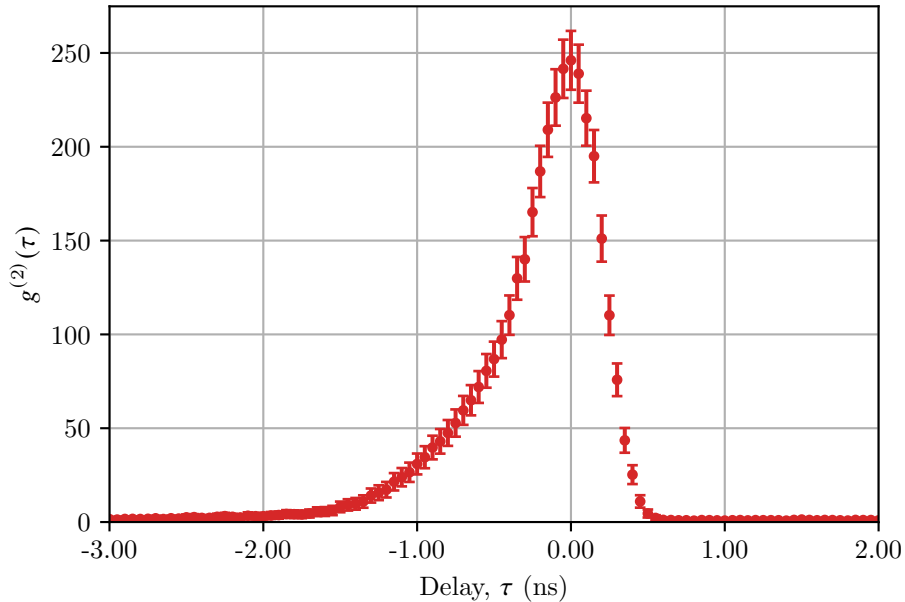


Figure 3.5: Normalized cross-correlation between detection events on the SNSPD for the signal photons and Si APD for the idler photons, after Type-0 SPDC. The FWHM of the coincidence distribution is 600 ps.

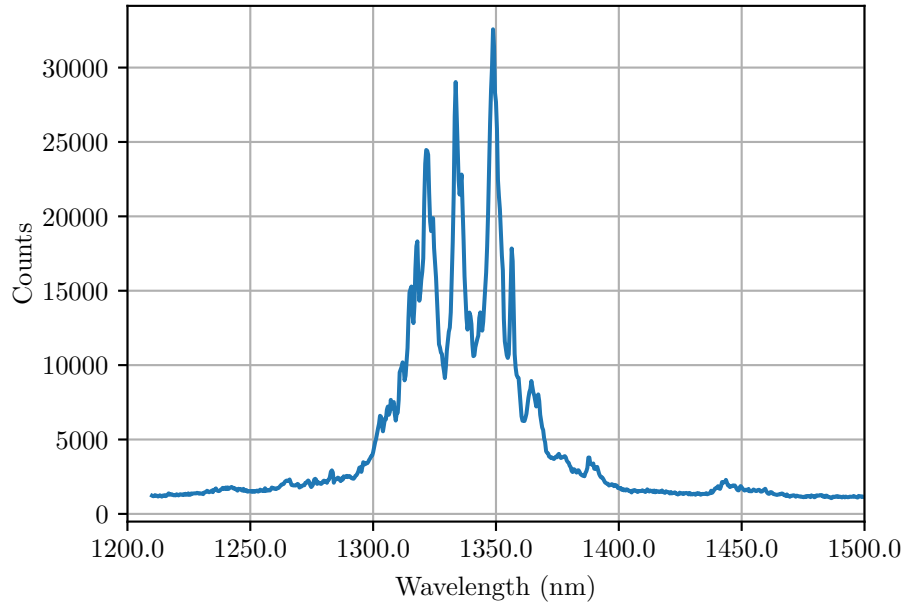


Figure 3.6: Wavelength distribution of signal photons after Type-II SPDC with 401 nm pump beam from ECDL. The spectrum is clearly multimodal with multiple prominent peaks at 1322 nm, 1334 nm, and 1349 nm, as well as several other smaller peaks. The spectrometer resolution is 1.0 nm. Detection of photon arrival events is performed using SNSPD.

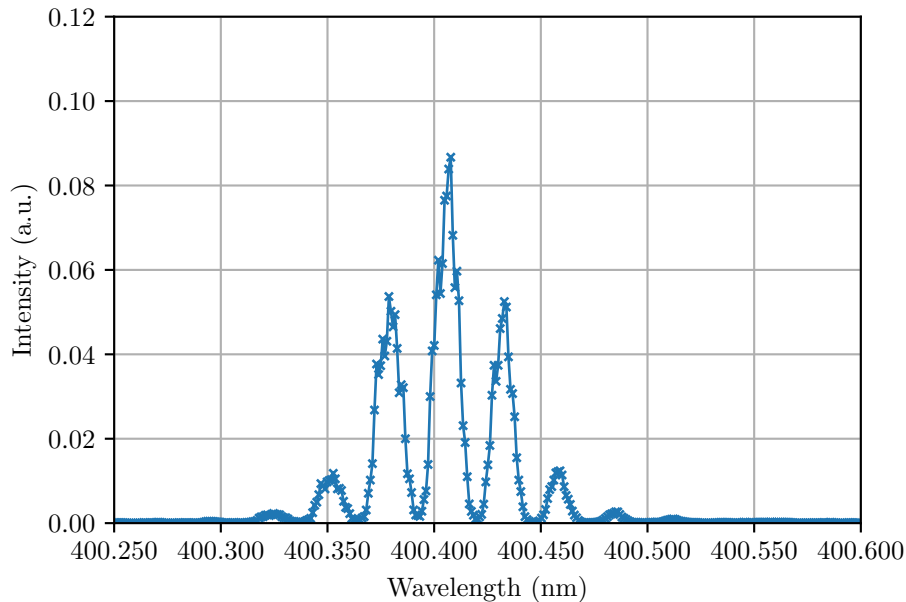


Figure 3.7: Spectrum of pump laser ECDL measured using spectrometer of resolution of < 1.0 parts per million. The spectrum is multimode with a peak center wavelength of 400.407 nm.

3.2 Type-0 SPDC

Phase matching at multiple wavelengths arising from the multimode nature of the laser can be mitigated by using a sufficiently single linewidth laser. The multimode Nichia laser diode is swapped out for the Ondax CP-405-PLR-40-4 laser diode, which is specified to have a center wavelength of 405 ± 0.5 nm and 160 MHz bandwidth using integrated volume Bragg grating.

A Type-0 SPDC down-conversion is performed using a different PPKTP crystal of poling period $\Lambda = 3.875$ μm in the same experimental setup, with phase matching conditions satisfied for a calculated oven temperature near 50°C for,

$$405 \text{ nm (o)} \rightarrow 1310 \text{ nm (o)} + 586 \text{ nm (o)}.$$

The longpass color glass filter (Schott OG-530) was additionally removed from the experimental setup due to the presence of fluorescence that increased the background count rate on the Si APD. The InGaAs APD, which has poor responsivity with respect to the 405 nm pump wavelength that is coupled into the optical fiber together with the signal photons, is used instead of the SNSPD for the photodetection of the signal photons.

3.2.1 Results and discussion

The actual oven temperature after optimization for heralding efficiency is $38.7 \pm 0.1^\circ\text{C}$, with the heralding efficiency averaging around 8% obtained with the Type-0 SPDC. The $g^{(2)}$ cross-correlation has a jitter of 625 ps, as shown in Figure 3.8, which means the total jitter of the cross-correlation is still dominated by the jitter of the silicon APD.

The wavelength spectrum of the pump laser is again characterized using the high-resolution spectrometer (Bristol Model 771), as shown in Figure 3.9, in order to verify single mode operation. The center wavelength of the pump beam is 405.033 nm with a FWHM of 0.002 nm (frequency bandwidth of 3.7 GHz), which is single mode operation.

The spectra of the signal and idler photons obtained is shown in Figure 3.10a and in Figure 3.10b, respectively. The measurements of bandwidth for both signal and idler are limited by the resolution of the respective spectrometer. The desired sub-THz bandwidth regime for the signal is achieved, since the 1.0 nm bandwidth (175 GHz frequency bandwidth) of the signal photon is an upper bound to the actual wavelength bandwidth of the signal.

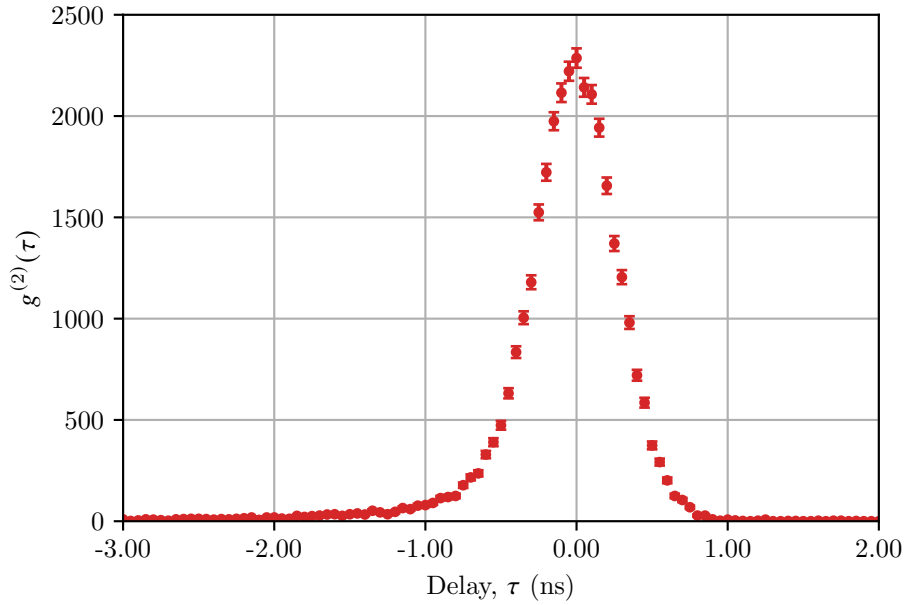


Figure 3.8: Cross-correlation between detection events on the InGaAs APD for the signal photons and Si APD for the idler photons, after Type-0 SPDC. The FWHM of the coincidence distribution is 625 ps.

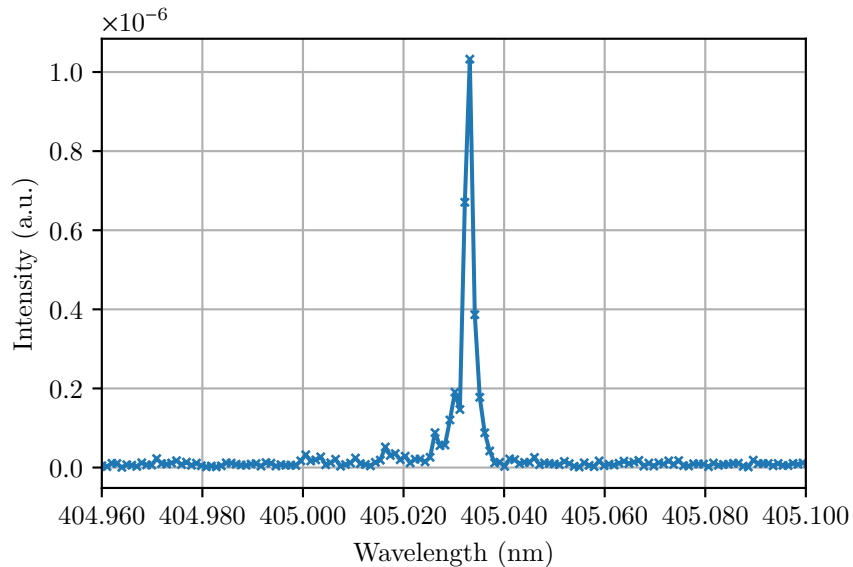
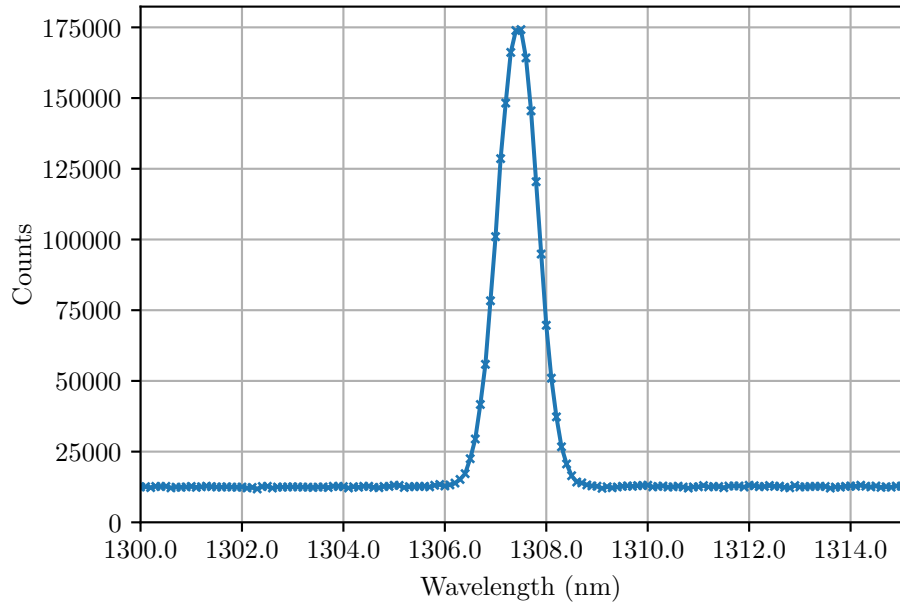
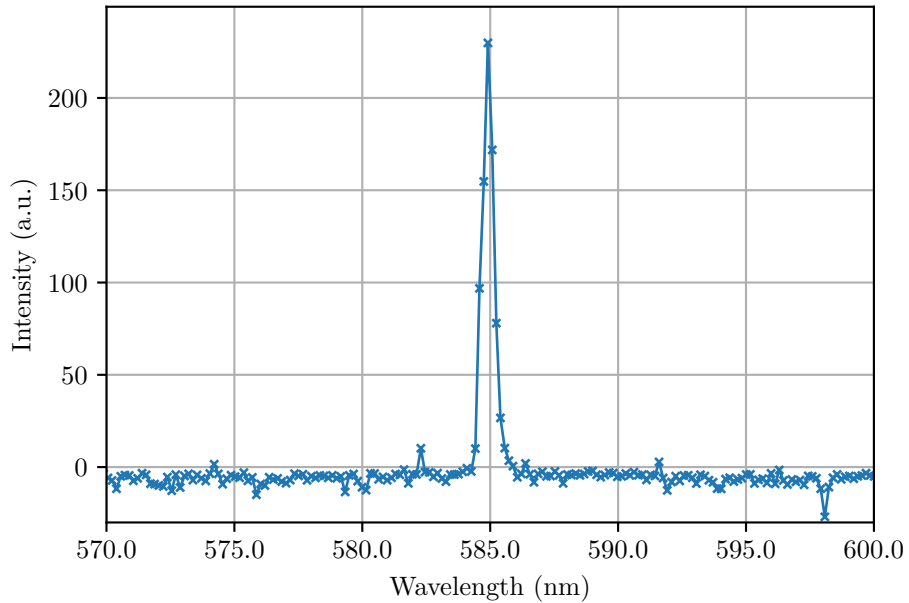


Figure 3.9: Spectrum of narrow bandwidth laser diode (Ondax CP-405-PLR-40-4) at a supplied laser current of 72.5 mA. The center wavelength is 405.033 nm with a FWHM of 0.002 nm.



(a) Wavelength distribution of signal photons centered at 1307.5 nm with a FWHM of approximately 1.0 nm. The rotating grating spectrometer of resolution 1.0 nm is used, and the photon detection counts are measured using the InGaAs APD.



(b) Wavelength distribution of idler photons centered at 584.9 nm with a FWHM of approximately 0.6 nm, measured using the OceanOptics spectrometer of resolution 0.5 nm.

Figure 3.10: Wavelength distribution of signal and idler photons after the Type-0 SPDC using 405 nm pump laser. Both spectra are limited by the resolution of the spectrometers.

Chapter 4

Conclusion

We started this thesis by proposing a highly non-degenerate spontaneous parametric down-conversion (SPDC) source of narrowband photon pairs in the sub-THz bandwidth regime in Chapter 1. The signal wavelength is centered at the zero-dispersion wavelength of SMF-28e optical fiber which is the most widely-deployed telecommunication fiber. A brief summary of how phase matching conditions for the down-conversion can be fulfilled using a combination of temperature tuning and quasi-phase matching is described in Chapter 2. In Chapter 3, we detailed the experimental setup necessary to facilitate the down-conversion of pump photons for both Type-II and Type-0 SPDC. The cross-correlation between the signal photon and idler photon detection events was measured to verify the presence of photon pairs. The wavelength distributions of the signal and idler photons were also plotted.

Multiple peaks in the distribution of the signal wavelength were present due to the multimode frequency of the pump laser used in the Type-II SPDC, even after using an external cavity for spectral filtering. The PPKTP crystal was then swapped out for a different poling period in order to obtain phase matching of Type-0 SPDC with a single mode pump laser, which yielded the desired single mode signal wavelength distribution near 1310 nm. The 1.0 nm FWHM of the signal wavelength envelope indicates that our photon pair source is within the desired sub-THz bandwidth regime, despite being limited by the resolution of the spectrometers.

Based on earlier calculations in Chapter 1, the total jitter measured for a photon pair source in this sub-THz bandwidth regime, with the signal wavelength centered at the zero-dispersion wavelength of SMF-28e, is on the order of sub-picoseconds, which is very promising for high time resolution applications in quantum communication.

4.1 Outlook

The wavelength distribution of the signal photons can be determined indirectly by measuring that of the idler photons to a sufficient accuracy — an etalon-based cavity can be built to measure the transmission of light as a function of the temperature-dependent resonant frequencies of the cavity, which can be shifted through the use of temperature tuning. This can potentially result in a spectral resolution of order of magnitudes better than the current CCD-based spectrometer. Sensitivity tests with varying temperature across the crystal can also be performed to verify long-term stability of the signal wavelength.

Subsequent entanglement of photon pairs, by introducing alternative down-conversion paths through the same crystal and recombining them, will serve as additional quantum resource for security in quantum communication applications.

References

- [1] J. Fekete, D. Rieländer, M. Cristiani, and H. de Riedmatten. Ultranarrow-band photon-pair source compatible with solid state quantum memories and telecommunication networks. *Phys. Rev. Lett.*, 110:220502, May 2013.
- [2] C. Clausen, F. Bussi eres, A. Tiranov, H. Herrmann, C. Silberhorn, W. Sohler, M. Afzelius, and N. Gisin. A source of polarization-entangled photon pairs interfacing quantum memories with telecom photons. *New Journal of Physics*, 16(9):093058, sep 2014.
- [3] P. G. Kwiat, K. Mattle, H. Weinfurter, A. Zeilinger, A. V. Sergienko, and Y. Shih. New high-intensity source of polarization-entangled photon pairs. *Phys. Rev. Lett.*, 75:4337–4341, Dec 1995.
- [4] P. G. Kwiat, E. Waks, A. G. White, I. Appelbaum, and P. H. Eberhard. Ultrabright source of polarization-entangled photons. *Phys. Rev. A*, 60:R773–R776, Aug 1999.
- [5] K. Hong, S. Baek, O. Kwon, and Y. Kim. Dispersive broadening of two-photon wave packets generated via type-i and type-ii spontaneous parametric down-conversion. *Journal of the Korean Physical Society*, 73:1650–1656, dec 2018.
- [6] A. Lenhard, M. Bock, C. Becher, S. Kucera, J. Brito, P. Eich, P. M uller, and J. Eschner. Telecom-heralded single-photon absorption by a single atom. *Phys. Rev. A*, 92:063827, Dec 2015.
- [7] K. Niizeki, K. Ikeda, M. Zheng, X. Xie, K. Okamura, N. Takei, N. Namekata, S. Inoue, H. Kosaka, and T. Horikiri. Ultrabright narrow-band telecom two-photon source for long-distance quantum communication. *Applied Physics Express*, 11(4):042801, mar 2018.
- [8] A. Haase, N. Piro, J. Eschner, and M. W. Mitchell. Tunable narrowband entangled photon pair source for resonant single-photon single-atom interaction. *Opt. Lett.*, 34(1):55–57, Jan 2009.

-
- [9] X. Bao, Y. Qian, J. Yang, H. Zhang, Z. Chen, T. Yang, and J. Pan. Generation of narrow-band polarization-entangled photon pairs for atomic quantum memories. *Phys. Rev. Lett.*, 101:190501, Nov 2008.
- [10] F. König, E. J. Mason, F. N. C. Wong, and M. A. Albota. Efficient and spectrally bright source of polarization-entangled photons. *Phys. Rev. A*, 71:033805, Mar 2005.
- [11] M. T. Liu and H. C. Lim. Transmission of o-band wavelength-division-multiplexed heralded photons over a noise-corrupted optical fiber channel. *Opt. Express*, 21(25):30358–30369, Dec 2013.
- [12] F. Kaneda, K. Garay-Palmett, A. B. U'Ren, and P. G. Kwiat. Heralded single-photon source utilizing highly nondegenerate, spectrally factorable spontaneous parametric downconversion. *Opt. Express*, 24(10):10733–10747, May 2016.
- [13] Corning. Corning® smf-28® ultra optical fiber, product information. Technical report, Corning Incorporated, Corning, NY, 2014.
- [14] J. Lee, L. Shen, A. N. Utama, and C. Kurtsiefer. Absolute clock synchronization with a single time-correlated photon pair source over 10km. 2020.
- [15] N. I. Nweke, P. Toliver, R. J. Runser, S. R. McNown, J. B. Khurgin, T. E. Chapuran, M. S. Goodman, R. J. Hughes, C. G. Peterson, K. McCabe, J. E. Nordholt, K. Tyagi, P. Hiskett, and N. Dallmann. Experimental characterization of the separation between wavelength-multiplexed quantum and classical communication channels. *Applied Physics Letters*, 87(17):174103, 2005.
- [16] T. E. Chapuran, P. Toliver, N. A. Peters, J. Jackel, M. S. Goodman, R. J. Runser, S. R. McNown, N. Dallmann, R. J. Hughes, K. P. McCabe, J. E. Nordholt, C. G. Peterson, K. T. Tyagi, L. Mercer, and H. Dardy. Optical networking for quantum key distribution and quantum communications. *New Journal of Physics*, 11(10):105001, oct 2009.
- [17] Nicolaas Bloembergen. *Nonlinear Optics*. WORLD SCIENTIFIC, 4th edition, 1996.
- [18] R. W. Boyd. *Nonlinear Optics*. Academic Press, 2008.
- [19] C. Couteau. Spontaneous parametric down-conversion. *Contemporary Physics*, 59(3):291–304, Jul 2018.

- [20] T. Y. Fan, C. E. Huang, B. Q. Hu, R. C. Eckardt, Y. X. Fan, R. L. Byer, and R. S. Feigelson. Second harmonic generation and accurate index of refraction measurements in flux-grown KTiOPO_4 . *Appl. Opt.*, 26(12):2390–2394, Jun 1987.
- [21] K. Fradkin, A. Arie, A. Skliar, and G. Rosenman. Tunable midinfrared source by difference frequency generation in bulk periodically poled KTiOPO_4 . *Appl. Phys. Lett.*, 74(914), 1999.
- [22] S. Emanuelli and A. Arie. Temperature-dependent dispersion equations for KTiOPO_4 and KTiOAsO_4 . *Appl. Opt.*, 42(33):6661–6665, Nov 2003.
- [23] R. S. Bennink. Optimal collinear gaussian beams for spontaneous parametric down-conversion. *Phys. Rev. A*, 81:053805, May 2010.
- [24] P. Ben Dixon, Danna Rosenberg, Veronika Stelmakh, Matthew E. Grein, Ryan S. Bennink, Eric A. Dauler, Andrew J. Kerman, Richard J. Molnar, and Franco N. C. Wong. Heralding efficiency and correlated-mode coupling of near-ir fiber-coupled photon pairs. *Phys. Rev. A*, 90:043804, Oct 2014.
- [25] K. MacAdam, A. Steinbach, and C. Wieman. A narrow-band tunable diode laser system with grating feedback, and a saturated absorption spectrometer for Cs and Rb . *American Journal of Physics*, 60:1098–1111, 1992.

Appendix A

Alignment procedure for optical setup

Before alignment, ensure that the desired pump beam is already coupled into a single mode fiber. Single photon detectors for both down-converted output photons (signal and idler) should be available, along with a timestamp card for cross-correlation of detection events between the two detectors.

1. Collimate the pump light emitted from the single mode fiber. Mount the collimation system on a kinematic mount (with pitch and yaw degrees of freedom). Adjust the distance of the lens from the fiber until desired focus distance is obtained.
2. Reflect the beam off a mirror mounted on another kinematic mount. Using two iris apertures on the same horizontal level and equidistant from the center of the crystal, adjust both mounts such that the beam passes through both irises. Ensure that the beam path also falls along the position of the crystal in the oven holder (that has pitch and roll degrees of freedom, e.g. a kinematic platform mount atop a rotation stage).
3. At the desired idler collection end, place another set of collimation system and mirror. The aspheric lens in the collimation system should be mounted on a Z-translation stage for fine Z adjustment. Couple laser light from this end and repeat steps 1 and 2 for the same set of iris apertures.
4. Remove the laser light from the collection end and maximize the coupling of the pump beam into the collection fiber, by adjusting the kinematic mounts on the collection end, as well as the position of the collection aspheric lens.
5. Place the dichoric mirror in the path of the pump beam, and readjust the coupling into the idler collection end. Repeat steps 3 and 4 with the signal

collection end as well.

6. Place in the crystal in the oven holder. Adjust the crystal such that the backreflection from the crystal aperture overlaps the incident path of the pump beam. Add an optional filter after the crystal to filter out the pump beam, and do the same backreflection adjustment.
7. Couple the collection output fibers to single photon detectors connected to the same timestamp card. Repeat the optimizations in step 4 for both signal and idler collection ports, maximizing the heralding efficiency.